applied optics

Heterodyne period measurement in a scanning beam interference lithography system

Shan Jiang,[1] Bo Lü,[2] Ying Song,[3] Zhaowu Liu,[1] Wei Wang,[1] Li Shuo,[1] and Bayanheshig[1,*]

[1]National Engineering Research Centre for Diffraction Gratings Manufacturing and Application, Changchun Institute of Optics, Fine Mechanics and Physics, Chinese Academy of Sciences, Changchun Jilin 130033, China
[2]First Department of Space Optics, Changchun Institute of Optics, Fine Mechanics and Physics, Chinese Academy of Sciences, Changchun Jilin 130033, China
[3]College of Instrumentation and Electrical Engineering, Jilin University, Changchun 130012, China
*Corresponding author: bayin888@sina.com

Received 30 March 2020; revised 30 May 2020; accepted 1 June 2020; posted 2 June 2020 (Doc. ID 393865); published 1 July 2020

The interference fringe period is an important phase-locking parameter in the scanning beam interference lithography (SBIL) system. To measure the interference fringe period accurately, a heterodyne period measurement method is proposed. Compared with traditional methods, the requirements for the stage motion characteristics are greatly reduced. In this paper, the theoretical error of the period measurement method is analyzed and relevant experiments are performed. The results show that the average period measurement value is 555.539 nm and the standard deviation of measurement repeatability is 2.5 pm. This method is significant for holographic grating fabrication using the SBIL system. © 2020 Optical Society of America

https://doi.org/10.1364/AO.393865

1. INTRODUCTION

Diffraction gratings are used widely in many areas of science and technology. To produce large-area linear diffraction gratings with high phase fidelity and uniform line widths, researchers at the Space Nanotechnology Laboratory of the Massachusetts Institute of Technology (MIT) developed the scanning beam interference lithography (SBIL) system [1–6]. In this system, two small coherent Gaussian laser beams interfere to produce a grating image on the substrate; the substrate then performs a stepping and scanning motion to enable exposure of large-scale gratings. Because the interference pattern formed by the coherence of the small-sized Gaussian beams has a Gaussian intensity envelope, the adjacent scans must partially overlap to create a uniform exposure dose, as illustrated in Fig. 1.

To compensate for the stage motion error in the step direction and complete the phase stitching of the overlapped part, Konkola [1] designed a dynamic phase-locking system for SBIL. Their dynamic phase-locking system converted the substrate displacement into an amount of phase change and then compensated for the phase change caused by this substrate displacement using an acousto-optic modulator (AOM). The interference fringe period is an important parameter in the process of conversion between the substrate displacement and the grating phase in this phase-locking system. To stitch the scans precisely, it is necessary to measure the fringe period with high accuracy. The effects of the period measurement error on the dose contrast and grating groove were analyzed in [7,8]. When the interference fringe period measurement accuracy is less than 176 ppm, the impact is small and makes it possible to meet the system requirements.

Measuring the exposure grating period using a scanning electron microscope (SEM) or an atomic force microscope (AFM) is a slow and inaccurate approach. Limited by the resolution of SEM and AFM, it is difficult to meet the needs of picometers of period measurement resolution. The displacement of the stage is measured by the displacement measuring interferometer (DMI) when phase locking and phase stitching. Using the same displacement measurement instrument, as when fringe stitching, can eliminate errors caused by the inconsistency of the displacement measurement instrument. Therefore, it is necessary to measure the periods of the interference fringes accurately using the same interferometer during exposure. Chen proposed a period measurement method that used a beam splitter (Fig. 2) [2,3].

In this method, the period measurement beam splitter is placed on the stage, and the exposure beams on both sides are reflected by the splitting surface and then transmitted to form an interference spot. The position sensing detector (PSD) detects the intensity change in the spot when the beam splitter moves in the step direction. The period of the change in the intensity with the change in the displacement of the beam splitter that is detected using the PSD is the period of the interference fringe.

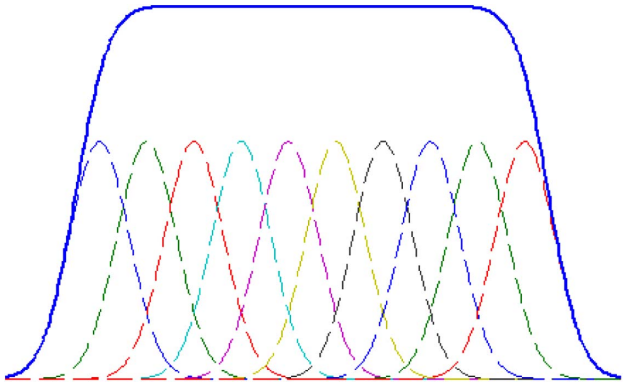

Fig. 1. Beam overlapping to create a uniform exposure dose.

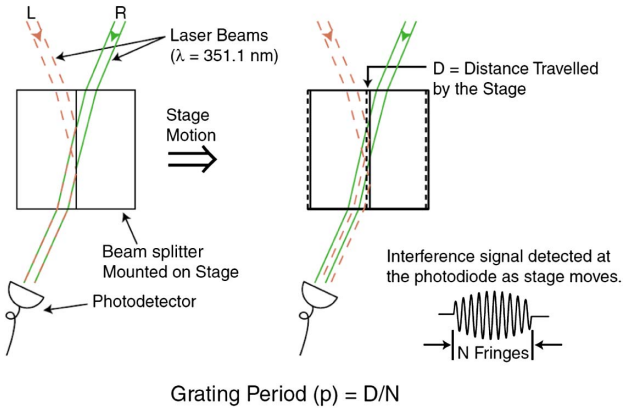

Fig. 2. Beam-splitter period measurement scheme [2].

To calculate the period accurately and reduce the effects of noise on the displacement and the intensity, Chen counted a large number N of fringes over a long-distance S, and the period p was then given by

$$p = \frac{S}{N}. \tag{1}$$

Chen used a fringe counting method to calculate the data for the start and the end of the beam-splitter motion [3], which required multipoint averaging of the data collected at the start and end positions to reduce the influence of the noise on the calculated results. The period measurement repeatability is demonstrated at 2.8 ppm. This method requires high XY stage positioning accuracy. The positioning accuracy of the air-bearing XY stage used by Chen was 30 nm [2]. However, it is too difficult to achieve such high positioning accuracy when using a large-stroke stage. Therefore, in our previous work, we proposed a method to assist the measurement of the period that used a short-stroke high-precision stage to reduce the positioning accuracy requirements for the XY stage, and the period measurement repeatability reached 10.8 ppm [9]. We applied a discrete Fourier transformation (DFT) algorithm to analyze the frequency spectrum of the signal and then calculated the period value using the main frequency [10]. However, the DFT algorithm acquires the signal sampling interval as a constant, and a large amount of zero-padding of the data is required to improve the resolution. The repeatability reached 17.5 ppm calculated by this method [10].

Joo used a Fresnel zone plate rather than a beam splitter to perform the fringe period measurements [11,12]. In [12], the author used two period measurement modes, i.e., the homodyne mode and the heterodyne mode, where the data collection and calculation method for the homodyne mode is similar to that of Chen. In the heterodyne mode, because the detected signal is weak, he used a lock-in amplifier that required use of a phase-locked loop, but the measurement repeatability for both algorithms was only one part per thousand, which cannot meet the system's requirements.

Xiang *et al.* used an updated metrology frame [13]. The authors normalized the measurement signal amplitude variations caused by movement of the beam splitter during the period measurement procedure and calculated the period value using a least-squares sine fitting algorithm. The final calculated repeatability reached 2.6 ppm. Xiang *et al.* later proposed the scanning reference grating (SRG) method, which is used to obtain the phase shift signal when scanning in the interference field [14]. This method can measure an interference field with a period value of 833.335 nm ± 10 pm over a 60 mm range. However, the SRG method is only suitable for relatively large-sized interference fields and is not suitable for measurement of the fringe periods of interference fields with a diameter of approximately 2 mm in the scanning interference field.

In this paper, the heterodyne fringe period measurement method is proposed. Based on the theory of Gaussian beam propagation, a theoretical analysis of the variation in the intensity caused by the motion of the beam splitter is performed. The heterodyne measurement approach has advantages that include insensitivity to amplitude changes, a strong anti-interference capability, and easy subdivision of the required electronics. The frequency difference between the two interference beams can be set easily to realize the heterodyne period measurement. The phase data obtained via the heterodyne measurement method is proportional to the displacement of the beam splitter. The phase data can then be fitted in a linear manner to calculate the fringe period. This calculation method is both simple and fast. Additionally, the heterodyne fringe period measurement method does not require the stage to have high positioning accuracy and low-speed motion characteristics, meaning that the demands for the stage motion characteristics can be greatly reduced. The proposed method is analyzed and verified by performing relevant experiments and will be of major significance for the fabrication of high-quality holographic gratings for use in SBIL systems.

2. PRINCIPLE OF PERIOD MEASUREMENT

The two exposure beams at the system wavelengths are incident on the grating substrate from opposing sides, and the angles between the two exposure beams and the normal of the grating substrate surface are denoted by θ_1 and θ_2. The interference fringe period p in the interference field is known from beam interference theory and can be written as

$$p = \frac{\lambda}{\sin\theta_1 + \sin\theta_2}. \tag{2}$$

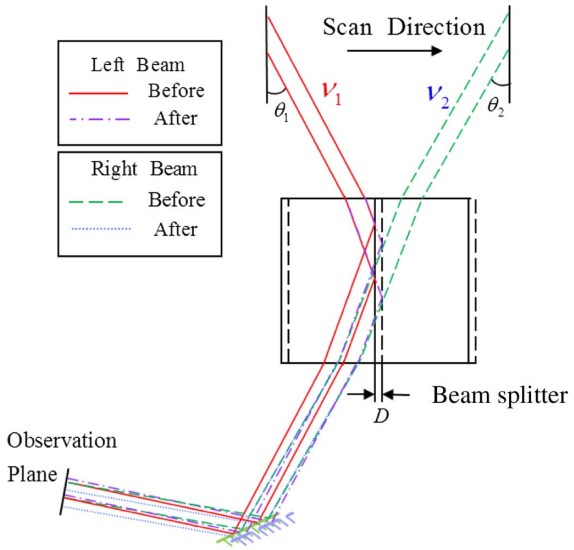

Fig. 3. Beam-splitter-based period measurement scheme.

Figure 3 shows a schematic diagram of the procedure for measurement of the interference fringe period. The splitting surface of the beam splitter is oriented perpendicular to the grating substrate. The angles between the exposure beam and the splitting surface on the two sides are θ_1 and θ_2, as noted above. During the period measurement, the beam splitter is used to overlap the two exposure beams spatial modes, i.e., the reflected light from the exposure beam on the left coincides with the transmitted light from the exposure beam on the right; this light is then folded via the plane mirror to form an interference pattern on the observation plane. The observation plane remains still when the stage carrying the beam-splitter mirror assembly is moving. The optical path differences and positions of the two beams that are incident on the observation plane change; further, the intensity distribution and phase of the interference pattern that are formed on the detector surface also change when the beam splitter moves along the step direction. By using the detector to measure the intensity variations in the interference pattern at the observation plane and analyzing the variation between the light intensity incident on the detector and the displacement of the beam splitter, the period value of the interference fringe can be determined.

3. RELATIONSHIP BETWEEN INTENSITY SIGNAL AND INTERFERENCE FRINGE PERIOD

Assuming that the splitting surface of the beam splitter lies perpendicular to the grating substrate surface, and that the normal of the splitting surface lies parallel to the step direction, the angles of incidence of the exposure beams on the left and right sides are θ_1 and θ_2, respectively, and the angle between the plane mirror and the grating substrate surface is φ. The angle between the observation plane and the surface of the grating substrate is β. The centroids of the two Gaussian beams coincide on the observation plane before the beam splitter moves. Figure 4 is a schematic diagram that illustrates the changes in the position and the optical path of the center of the Gaussian beam on the two arms when the beam splitter moves by displacement D in

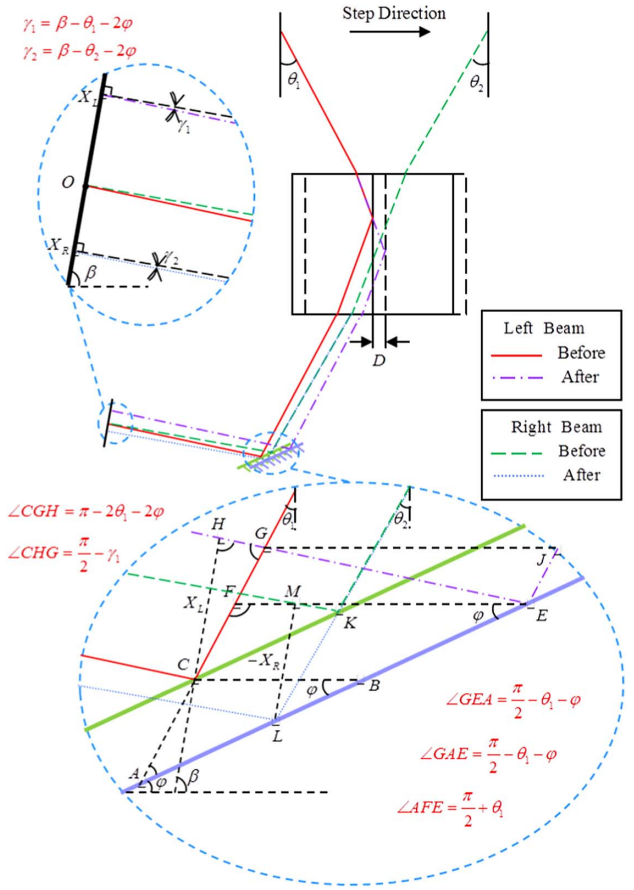

Fig. 4. Ray tracing illustrating the movement of the Gaussian beam centroids.

the step direction. The position changes in the centroids of the two Gaussian beams when they reach the detector are calculated as follows:

$$X_L = \overline{CH} = \frac{2D\cos\varphi\cos(\theta_1+\varphi)}{\cos(\beta-2\varphi-\theta_1)}, \tag{3}$$

$$X_R = \overline{ML} = -\frac{2D\sin\varphi\sin(\theta_2+\varphi)}{\cos(\beta-2\varphi-\theta_2)}. \tag{4}$$

This indicates that the movement of the beam-splitter mirror assembly causes the positions of the centroids of the Gaussian beams incident on the observation plane to move in opposite directions, and the coincidence of the spots on which the two beams are incident on the observation plane decreases.

After the calculation, the complex amplitude distribution of the two beams when superimposed on the observation plane is given by

$$\begin{aligned} E_O(x,y,D,t) &= A_L \exp\left[-\frac{(x-X_L)^2+y^2}{\omega_L^2}\right]\exp(-i\phi_L(x,y,D,t)) \\ &+ A_R \exp\left[-\frac{(x-X_R)^2+y^2}{\omega_R^2}\right]\exp(-i\phi_R(x,y,D,t)), \end{aligned} \tag{5}$$

where

$$\begin{cases} \phi_L(x, y, D, t) = k\left[z_L + \frac{(x-X_L)^2+y^2}{2R_L}\right] - \arctan\left(\frac{z_{L0}}{b_L}\right) + 2\pi\nu_1 t \\ \phi_R(x, y, D, t) = k\left[z_R + \frac{(x-X_R)^2+y^2}{2R_R}\right] - \arctan\left(\frac{z_{R0}}{b_R}\right) + 2\pi\nu_2 t \\ z_L(x, y, D) = z_{L0} + \Delta_L + (x-X_L)\sin(\beta-2\varphi-\theta_1) \\ z_R(x, y, D) = z_{R0} + \Delta_R + (x-X_R)\sin(\beta-2\varphi-\theta_2) \\ \Delta_L(D) = \frac{2D\cos\varphi\sin(\beta-\varphi)}{\cos(\beta-2\varphi-\theta_1)} \\ \Delta_R(D) = \frac{2D\sin\varphi\cos(\beta-\varphi)}{\cos(\beta-2\varphi-\theta_2)} \end{cases}. \quad (6)$$

Here, b is the confocal parameter of the laser beam, R is the radius of curvature of the wavefront at z, ν ($|\nu_2 - \nu_1| \ll \nu_1$) is the light wave frequency, and z_{L0} and z_{R0} are the optical path length from the centroids of the beam on the two sides to the waist position; further, Δ_L is the optical path length change of the left beam centroid, and Δ_R is the optical path length change of the right beam centroid. Because the two beams are staggered on the observation plane in tandem with the movement of the beam splitter, a lens with focal length F is added behind the observation plane; further, the observation plane is located on the front focal plane of the lens, and the detector is located on the rear focal plane of the lens. According to Fourier optics theory, the light wave distribution on the rear focal plane of the lens is a Fourier transform of the light wave distribution on the front focal plane, as shown by the following formula:

$$E_s(f_x, f_y, D, t)\big|_{f_x=\frac{x}{\lambda F}, f_y=\frac{y}{\lambda F}} = \mathrm{FT}(E_O(x, y, D, t)). \quad (7)$$

The intensity distribution on the rear focal plane is

$$I_s(x, y, D, t) = E_s(f_x, f_y, D, t) \times E_s^*(f_x, f_y, D, t)\big|_{f_x=\frac{x}{\lambda F}, f_y=\frac{y}{\lambda F}}. \quad (8)$$

After it passes through the lens, the light spot is then focused on the rear focal plane. The focused spot is small. Assuming that the signal can then be detected by the detector, the signal that is received by the detector becomes the integral of the light intensity distribution. Because the light paths of the exposure beams on the two sides are symmetrical, it is assumed that $\omega_L = \omega_R = \omega$, $b_L = b_R = b$, and $R_L = R_R = R$. This means that the signal detected by the detector can be given as

$$S(D, t) = \frac{\pi\omega^2\lambda^2F^2}{2}\left(A_L^2 + A_R^2\right) + \pi\omega^2A_LA_R\lambda^2F^2 \times \exp\left[-\frac{(\pi\omega)^2(\sin\gamma_1 - \sin\gamma_2)}{2\lambda^2} - \frac{1}{2}\left(\frac{X_L - X_R}{\omega}\right)^2\right]\cos(\varphi_S), \quad (9)$$

where

$$\begin{cases} \varphi_S = \varphi_D(D) + \varphi_t(t) + \varphi_c \\ \varphi_c = k(z_{L0} - z_{R0}) - \arctan\left(\frac{z_L}{b}\right) + \arctan\left(\frac{z_R}{b}\right) \\ \varphi_t(t) = 2\pi(\nu_1 - \nu_2)t \\ \varphi_D(D) = \frac{k}{2}(X_L - X_R)(\sin\gamma_1 + \sin\gamma_2) - k(\Delta_L - \Delta_R) \\ \qquad = 2\pi\frac{D(\sin\theta_1+\sin\theta_2)}{\lambda} + \frac{4\pi D\cos(\theta+\gamma)}{\lambda\cos\gamma}\sin^2\delta \end{cases}. \quad (10)$$

When the beam frequencies on the two sides are equal, i.e., $\nu_1 = \nu_2$, the relationship between the signal intensity at the detector at time t and the displacement of the beam splitter can be obtained using the formulas given in Eqs. (9) and (10), as shown in Fig. 5. Figure 5(b) shows an enlargement of the central area between the two dashed lines, which is indicated by the dashed line in Fig. 5(a).

Figure 5 shows that the light intensity signal received at the detector is a cosine function that has a specific envelope with respect to the beam-splitter displacement D. The reason for this spindle-shaped envelope is that, as the beam splitter moves, the coherent light spot on the detector is gradually staggered, and, because of the Gaussian intensity distribution of the light spot, the cosine variation of the signal decreases.

Substitution of Eq. (2) into Eq. (10) gives

$$p = \frac{2\pi D}{\varphi_D(D)}\left[1 - \frac{2\cos(\theta+\gamma)}{\cos\gamma(\sin\theta_1 + \sin\theta_2)}\delta^2 - \frac{1}{k\left(b + z^2/b\right)}\right], \quad (11)$$

where

$$\begin{cases} \theta = \frac{\theta_1+\theta_2}{2} \\ \delta = \frac{\theta_1-\theta_2}{2} \\ k = \frac{2\pi}{\lambda} \end{cases}. \quad (12)$$

By appropriate beam alignment, which has been published in our previous work [15], δ can be guaranteed to be better than 100 μrad, and then the second term of Eq. (11) is better than 10^{-8}. The beam waist radius of the exposure beam is 1.3 mm, and the wavelength is 413.1 nm. Calculations show that the third term in Eq. (11) is of the order of 10^{-8}. Therefore, the last two terms in Eq. (11) can be omitted and the equation simplified to read

$$p = \frac{2\pi D}{\varphi_D(D)}. \quad (13)$$

Equation (13) thus shows that the period of the interference fringe can be obtained using $\varphi_D(D)$ and D.

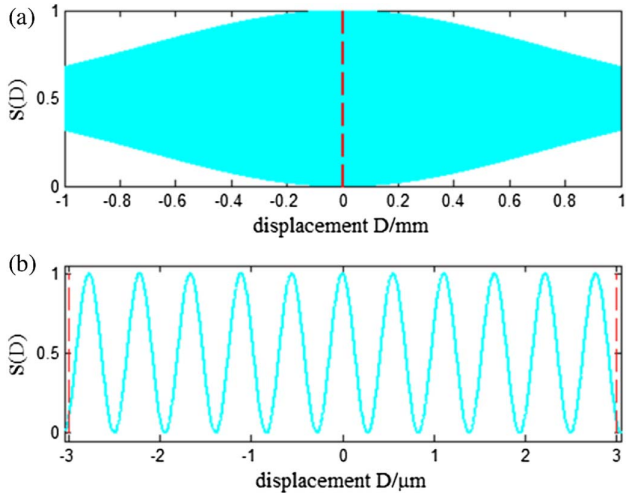

Fig. 5. (a) Relationship between the detector power signal and the beam-splitter displacement. (b) Enlarged view of the central area between the two dashed lines indicated by the dashed line in (a).

4. HETERODYNE PERIOD MEASUREMENT

Figure 6 shows a schematic diagram of the process for measurement of the difference frequency period. The SBIL system contains two AOMs, which are located in the exposure light paths on both sides; these AOMs are used to generate a specific frequency modulation that is convenient for phase locking. At the beginning of the exposure process, the frequencies of the AOMs on the two sides are set to be equal, and both AOMs are set to a frequency of 122 MHz. During exposure, the corresponding frequency can be adjusted to lock the interference fringes dynamically. The heterodyne period measurement performed before exposure. During the heterodyne period measurement, the two AOMs are set at different frequencies. The frequency setting of AOM1 is 123 MHz and the frequency setting of AOM2 is 121 MHz, i.e., there is a frequency difference of 2 MHz between the sides. During the period measurement, part of the light from the exposure beams incident on both sides is adjusted to coincide and enters into the phase receiver (PR1). As a reference signal for the differential frequency measurement, the phase change in the reference signal with time can be written as

$$\Phi_R(t) = 2\pi(\nu_1 - \nu_2)\, t. \tag{14}$$

After the exposure beams pass through the beam splitter and overlap, the combined beam enters the second phase receiver (PR2). This is used as the measurement signal, and Eqs. (10) and (11) show that, when the beam splitter moves by D, the phase change is

$$\Phi_M(D, t) = \varphi_D(D) + 2\pi(\nu_1 - \nu_2)\, t. \tag{15}$$

By combining Eqs. (14) and (15), we obtain

$$\varphi_D(D) = \Phi_M(D, t) - \Phi_R(t)\,. \tag{16}$$

As shown in Fig. 6, the reference signal is received by phase receiver PR1, and the measurement signal is received by phase receiver PR2. The preceding analysis shows that, with movement of the beam splitter, a change in the amplitude of the light intensity signal will appear in the form of a spindle-shaped envelope, and the heterodyne period measurement is performed using the AC measurement system, which overcomes the effects of beam intensity fluctuations and has a strong anti-interference capability. The phase receiver converts the detected sinusoidal light intensity change into an electrical signal, which is then converted into a square wave signal at the same frequency using a back-end circuit. To improve the measurement accuracy, the signal is generally subdivided electronically inside the measurement calculation unit to improve the measurement resolution and the measurement accuracy. The schematic diagram of data processing is shown in Fig. 7. n times subdivision is realized, that is, when the beam splitter displacement D changes by a fringe period p, P_m changes by n. A digital signal, P_m, is finally obtained:

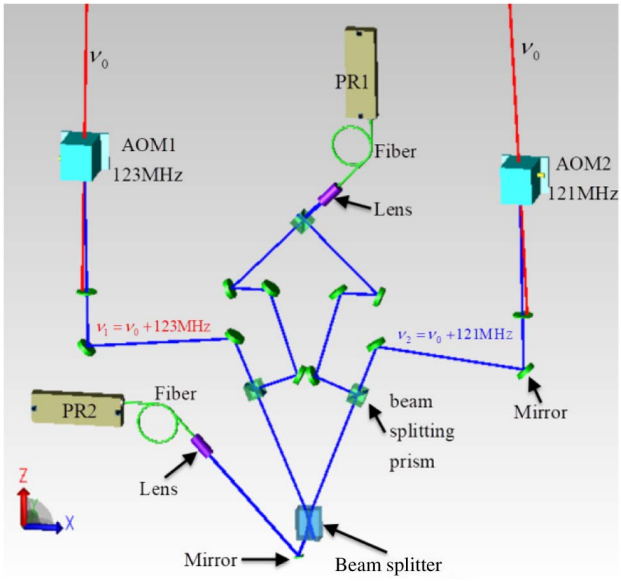

Fig. 6. Heterodyne period measurement concept.

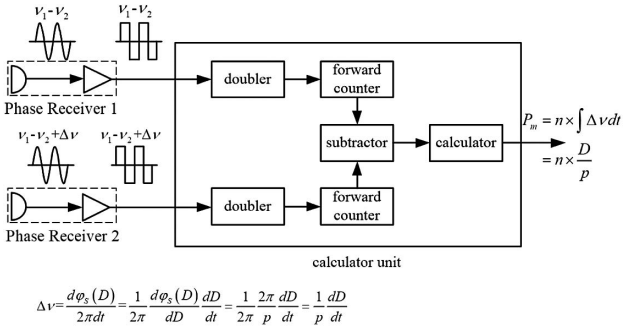

Fig. 7. Schematic diagram of data processing principle.

$$P_m(D) = n \times \frac{D}{p}. \tag{17}$$

Equation (17) shows that the phase measurement digital signal P_m is proportional to the displacement D. Period measurements can collect the displacement and phase measurement data during the movement of the beam splitter, and straight line fitting is then performed on the displacement and phase measurement data to obtain the slope S_k, which can be used to calculate the period as follows:

$$p = \frac{n}{S_k}. \tag{18}$$

This calculation method is simple and fast and also avoids the problem of correction of the light intensity changes during the same frequency period measurement. In addition, it is not necessary to average the start and end positions when using this approach; further, the stage is not required to have extremely high positioning accuracy.

5. EXPERIMENT

In the experiment, the laser wavelength was 413.1 nm, the beam waist radius at the interference fringe was 1.3 mm, the angle of incidence of the beams on both sides was 21.8°, and the nominal fringe period was 555.53 nm. The beam alignment process makes $\delta \leq 10$ μrad [15]. The phase receiver selected was the Agilent 10780F remote receiver with a 9 mm lens on the fiber optic cable input and the number of phase receiver counts

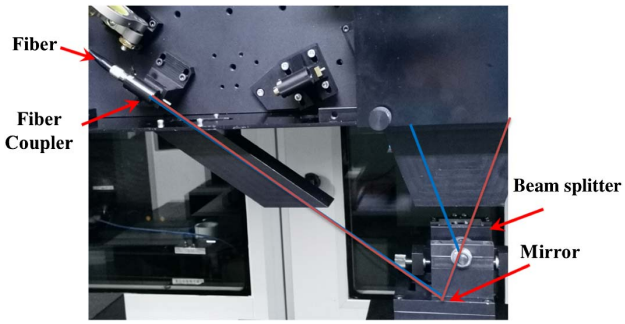

Fig. 8. Picture of the beam splitter and the period measurement structure.

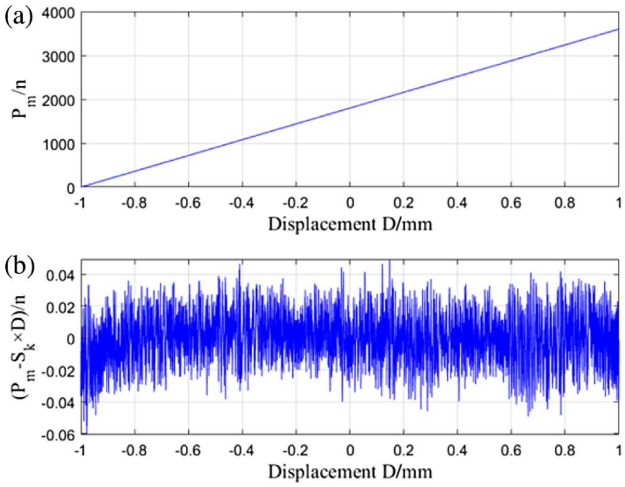

Fig. 9. (a) Period measurement data. (b) Measurement data with the slope removed.

per fringe period was 1024. The stage displacement measurements were performed using an interferometer with resolution of 0.15 nm. Figure 8 shows the beam splitter and measurement structure used in the heterodyne period measurement experiment.

The stage displacement measurements and heterodyne phase measurements were also performed using Agilent products to enable synchronous data acquisition. The data sampling frequency was 20 kHz. The table movement speed during the period measurement was 100 μm/s, and the movement distance was 2 mm. The measurement data are presented in Fig. 9(a). The abscissa in Fig. 9 is the displacement of the beam splitter measured by the interferometer. The ordinate is the ratio of the heterodyne measurement digital signal P_m to the subdivision number n, as can be seen in Eq. (17), the P_m/n is the number of fringe periods. The data after the slope was removed are shown in Fig. 9(b). Noise in the residual was caused predominantly by the phase receiver noise, shot noise, and displacement interferometer noise.

The measured data were fitted once to obtain the slope S_k, which was then substituted into Eq. (18) to obtain the period measurement value. The average of 20 measurements was taken to obtain the period measurement average value of 555.539 nm and the repeatability was 2.5 pm (σ value of 4.5 ppm).

6. CONCLUSION

The interference fringe period is an important parameter for the scanning interference field exposure system. The measurement accuracy of this period determines the phase stitching accuracy when the exposure grating is exposed. To measure the interference fringe period formed by two-beam interference accurately in the SBIL system, this paper proposes a heterodyne period measurement approach. This paper also provides analysis of the theoretical error of this method, and relevant experiments are performed. The following conclusions can be drawn from this work: (1) the theoretical relative error of the proposed method using the movement of the beam splitter is of the order of 10^{-8}, which meets the requirements for period measurement; (2) a frequency difference is introduced into the interfering beams, and the speed and stability requirements for table operation are reduced during the measurements; (3) the heterodyne period measurement method uses the data obtained during movement of the beam splitter to perform linear fitting during the calculation process, which shows higher accuracy than the fringe counting method and has a higher calculation speed; (4) the repeatability of the heterodyne period measurement from the experimental results reached 2.5 pm (σ value of 4.54 ppm), which can meet the needs of the exposure equipment.

When compared with the traditional method, the heterodyne period measurement method does not need to constrain either the positioning accuracy or the low-speed motion characteristics of the stage and greatly reduces the motion characteristics requirements of the stage. This method is more advantageous when the large-stroke, heavy-load stage cannot guarantee its low-speed motion performance, which is significant for the SBIL system when fabricating large-sized holographic gratings.

Funding. National Natural Science Foundation of China (NSFC) (61227901, 61905243, 61905245); Jilin Province Science & Technology Development Program Project in China (20190103157JH).

Acknowledgment. We thank H. Chen and Prof. Q. Chen for technical assistance with the two-axis air bearing stage.

Disclosures. The authors declare no conflicts of interest.

REFERENCES

1. P. T. Konkola, "Design and analysis of a scanning beam interference lithography system for patterning gratings with nanometer-level distortions," Ph.D. thesis (Massachusetts Institute of Technology, 2003).
2. C. G. Chen, "Beam alignment and image metrology for scanning beam interference lithography fabricating gratings with nanometer phase accuracy," Ph.D. thesis (Massachusetts Institute of Technology, 2003).
3. C. G. Chen, P. T. Konkola, R. K. Heilmann, G. S. Pati, and M. L. Schattenburg, "Image metrology and system controls for scanning beam interference lithography," J. Vac. Sci. Technol. B **19**, 2335–2341 (2001).
4. J. Montoya, "Toward nano-accuracy in scanning beam interference lithography," Ph.D. thesis (Massachusetts Institute of Technology, 2006).

5. Y. Zhao, "Ultra-high precision scanning beam interference lithography and its application—spatial frequency multiplication," Ph.D. thesis (Massachusetts Institute of Technology, 2008).
6. R. K. Heilmann, P. T. Konkola, C. G. Chen, G. S. Pati, and M. L. Schattenburg, "Digital heterodyne interference fringe control system," J. Vac. Sci. Technol. B **19**, 2342–2346 (2001).
7. S. Jiang, Bayanheshig, Y. Song, M. Pan, and W. Li, "Effect of measured interference fringe period error on groove profile of grating masks in scanning beam interference lithography system," Acta Opt. Sinica **34**, 0405003 (2014).
8. S. Jiang, Bayanheshig, W. Li, Y. Song, and M. Pan, "Effect of period setting value on printed phase in scanning beam interference lithography system," Acta Opt. Sinica **34**, 0905003 (2014).
9. S. Jiang, Bayanheshig, M. Pan, W. Li, and Y. Song, "An accurate method for measuring intererence fringe period in scanning beam interference lithography system," Acta Opt. Sinica **35**, 0705001 (2015).
10. S. Jiang, "Study on measurement and adjustment of interference fringes for scanning beam interference lithography system," Ph.D. thesis (Changchun Institute of Optics, Fine Mechanics and Physics, Chinese Academy of Sciences, 2015).
11. C. Joo, G. S. Pati, C. G. Chen, P. T. Konkola, R. K. Heilmann, and M. L. Schattenburg, "Precision fringe metrology using a Fresnel zone plate," J. Vac. Sci. Technol. B **20**, 3075–3079 (2002).
12. C. Joo, "Image grating metrology using a Fresnel zone plate," M.S. thesis (Massachusetts Institute of Technology, 2003).
13. X. Xiang, M. Li, C. Wei, and C. Zhou, "Precision fringe period metrology using an LSQ sine fit algorithm," Appl. Opt. **57**, 4777–4784 (2018).
14. X. Xiang, W. Jia, C. Xiang, M. Li, F. Bu, S. Zhu, C. Zhou, and C. Wei, "Long-range in situ picometer measurement of the period of an interference field," Appl. Opt. **58**, 2929–2935 (2019).
15. W. Wang, Bayanheshig, Y. Song, S. Jiang, and M. Pan, "Beam alignment and convergence analysis of scanning beam interference lithography systems," Chin. J. Lasers **34**, 0405003 (2014).

159.226.165.15 [at 2021-04-25 21:58:58]